

Thermal properties of monoclinic $\text{KLu}(\text{WO}_4)_2$ as a promising solid state laser host

Òscar Silvestre,¹ Joan Grau,² Maria Cinta Pujol,¹ Jaume Massons,¹ Magdalena Aguiló,¹ Francesc Díaz,¹ Mieczyslaw Tadeusz Borowiec,³ Andrzej Szewczyk,³ Maria Urszula Gutowska,³ Marta Massot,⁴ Agustín Salazar,⁴ and Valentin Petrov⁵

¹Física i Cristal·lografia de Materials (FiCMA), Universitat Rovira i Virgili, Campus Sescelades c/ Marcel·lí Domingo, s/n, 43007-Tarragona, Spain

²Departament de Mecànica de Fluids, CEIB, Universitat Politècnica de Catalunya c/ Compte d'Urgell, 187, 08036-Barcelona, Spain

³Institute of Physics, Polish Academy of Sciences, Al. Lotników 32/46, Pl 02-668, Warsaw, Poland

⁴Departamento de Física Aplicada I, Escuela Técnica Superior de Ingeniería, Universidad del País Vasco, Alameda Urquijo s/n, 48013 Bilbao, Spain

⁵Max-Born-Institute for Nonlinear Optics and Ultrafast Spectroscopy, 2A Max-Born-Str., D-12489, Berlin, Germany

*Corresponding author: mariacinta.pujol@urv.cat

Abstract: Thermal analysis of the monoclinic solid state laser host $\text{KLu}(\text{WO}_4)_2$ is presented. The specific heat was measured by the relaxation method in the temperature range from 1.9 to 385 K: its value at room temperature is 0.324 J/gK. The Debye temperature and the sound velocity amount to 303 ± 3 K and 3734 m/s. The linear thermal expansion tensor was measured by X-ray powder diffraction from room temperature up to 773 K. The eigenvalues of this tensor are $\alpha'_{11} = 8.98 \times 10^{-6} \text{ K}^{-1}$, $\alpha'_{22} = 3.35 \times 10^{-6} \text{ K}^{-1}$, and $\alpha'_{33} = 16.72 \times 10^{-6} \text{ K}^{-1}$, with the maximum value in the *a-b* crystallographic plane, at 31.94° from the N_g principal optical axis. The thermal diffusivity and its anisotropy in the temperature range between 300 and 500 K were measured by the pyroelectric method to determine the thermal conductivity tensor. The eigenvalues of the thermal conductivity are $\kappa'_{11} = 2.95 \text{ Wm}^{-1}\text{K}^{-1}$, $\kappa'_{22} = 2.36 \text{ Wm}^{-1}\text{K}^{-1}$, and $\kappa'_{33} = 4.06 \text{ Wm}^{-1}\text{K}^{-1}$, with the maximum value along a direction again in the *a-b* crystallographic plane, at 40.75° from the N_g principal optical axis. Simulation of the temperature distribution in a bulk sample of $\text{KLu}(\text{WO}_4)_2$ with dimensions $3 \times 3 \times 3 \text{ mm}^3$ shows that pump and laser beam directions along the N_p principal optical axis in terms of thermal effects are preferable because the propagation is along a quasi-isothermal path.

© 2008 Optical Society of America

OCIS codes: (140.3580) Lasers, solid-state; (120.6810) Thermal effects

References and links

1. A. A. Kaminskii, *Crystalline Lasers: Physical Processes and Operating Schemes*, (CRC Press, New York, 1996).
2. J. Liu, V. Petrov, X. Mateos, H. Zhang, and J. Wang, "Efficient high-power laser operation of $\text{Yb}:\text{KLu}(\text{WO}_4)_2$ crystals cut along the principal optical axes," *Opt. Lett.* **32**, 2016-2018 (2007).
3. X. Mateos, V. Petrov, J. Liu, M. C. Pujol, U. Griebner, M. Aguiló, F. Díaz, M. Galan, and G. Viera, "Efficient 2- μm continuous-wave laser oscillation of $\text{Tm}^{3+}:\text{KLu}(\text{WO}_4)_2$," *IEEE J. Quantum Electron.* **42**, 1008-1015 (2006).

4. U. Griebner, J. Liu, S. Rivier, A. Aznar, R. Grunwald, R. M. Sole, M. Aguilo, F. Diaz, and V. Petrov, "Laser operation of epitaxially grown Yb:KLu(WO₄)₂-KLu(WO₄)₂ composites with monoclinic crystalline structure," *IEEE J. Quantum Electron.* **41**, 408-414 (2005).
5. Ó. Silvestre, M. C. Pujol, M. Aguiló, F. Díaz, X. Mateos, V. Petrov, and U. Griebner, "CW laser operation of KLu_{0.945}Tm_{0.055}(WO₄)₂-KLu(WO₄)₂ epilayers near 2 μm," *IEEE J. Quantum Electron.* **43**, 257-260 (2007).
6. M. C. Pujol, X. Mateos, A. Aznar, X. Solans, S. Surinach, J. Massons, F. Diaz, and M. Aguilo, "Structural redetermination, thermal expansion and refractive indices of KLu(WO₄)₂," *J. Appl. Cryst.* **39**, 230-236 (2006).
7. W. Koechner and M. Bass, *Solid-State Lasers: A Graduate Text*, (Springer-Verlag, New York, 2003).
8. R. L. Aggarwal, D. J. Ripin, J. R. Ochoa, and T. Y. Fan, "Measurement of thermo-optic properties of Y₃Al₅O₁₂, Lu₃Al₅O₁₂, YAlO₃, LiYF₄, LiLuF₄, BaY₂F₈, KGd(WO₄)₂, and KY(WO₄)₂ laser crystals in the 80–300 K temperature range," *J. Appl. Phys.* **98**, 103514-1-14 (2005).
9. M. T. Borowiec, A. Szweczyk, T. Zayarnyuk, A. Pikul, D. Kaczorowski, E. E. Zubov, M. Gutowska, V. P. Dyakonov, M. Barański, H. Szymczak, M. C. Pujol, M. Aguiló, and F. Díaz, "The specific heat capacity and magnetic phase transitions for monoclinic rare earth double tungstate," submitted to *New J. Phys.* (2008).
10. J. Zhang, K. Wang, J. Wang, H. Zhang, W. Yu, X. Wang, Z. Wang, Q. Lu, and M. Ba, "Anisotropic thermal properties of monoclinic Yb:KLu(WO₄)₂ crystals," *Appl. Phys. Lett.* **87**, 061104-1-3 (2005).
11. Y. Sato and T. Taira, "The studies of thermal conductivity in GdVO₄, YVO₄, and Y₃Al₅O₁₂, measured by quasi-one-dimensional flash method," *Opt. Express* **14**, 10528-10536 (2006).
12. T. Kushida, "Linewidth and thermal shifts of spectral lines in neodymium-doped yttrium aluminum garnet and calcium fluorophosphates," *Phys. Rev.* **185**, 500-508 (1969).
13. X. Chen and B. Di Bartolo, "Temperature dependence of spectral linewidths and lineshifts of Nd³⁺ ions in CaY₂Mg₂Ge₃O₁₂ laser crystal," *J. Appl. Phys.* **75**, 1710-1714 (1994).
14. D. D. L. Chung, P. W. DeHaven, H. Arnold, and D. Ghosh, *X-ray Diffraction at Elevated Temperatures. A Method for In Situ Process Analysis*, (VCH, New York, 1993).
15. M. C. Pujol, X. Mateos, R. Solé, J. Massons, Jna. Gavalda, F. Díaz, and M. Aguilo, "Linear thermal expansion tensor in KRE(WO₄)₂ (RE = Gd, Y, Er, Yb) monoclinic crystals," *Mater. Sci. Forum* **378–381**, 710–715 (2001).
16. A. Authier (Ed.), *International Tables for Crystallography, Volume D: Physical Properties of Crystals* (The International Union of Crystallography, Kluwer Academic Publishers, Dordrecht/Boston/London, 2003).
17. M. Chirtoc, D. Dadarlat, D. Bicanic, J. S. Antoniow and M. Egée, *Progress in Photoacoustic and Photoacoustic Science and Technology* (vol 3, ed. by A Mandelis and P Hess, Bellingham, WA, SPIE Optical Engineering Press, 1997).
18. S. Delenclos, M. Chirtoc, A. H. Sahraoui, C. Kolinsky, and J. M. Buisine, "Assessment of calibration procedures for accurate determination of thermal parameters of liquids and their temperature dependence using the photopyroelectric method," *Rev. Sci. Instrum.* **73**, 2773-2780 (2002).
19. R. E. Hummel, *Electronic Properties of Materials*, (Springer-Verlag, New York, 1985).
20. I. V. Mochalov, "Laser and nonlinear properties of the potassium gadolinium tungstate laser crystal KGd(WO₄)₂:Nd³⁺-(KGW:Nd)," *Opt. Eng.* **36**, 1660-1669 (1997).
21. R. Gaumé, B. Viana, D. Vivien, J.-P. Roger, and D. Fournier, "A simple model for the prediction of thermal conductivity in pure and doped insulating crystals," *Appl. Phys. Lett.* **83**, 1355-1357 (2003).

1. Introduction

KLu(WO₄)₂ (hereafter KLuW) belongs to a class of compounds known as monoclinic potassium double tungstates, KREW, and similar to the other inert compounds of this kind, KGdW and KYW, it is well suited as a host for active rare-earth (RE) ion dopants [1]. Starting from 1979, this laser host has been demonstrated with Nd³⁺, Er³⁺, and Ho³⁺ doping [1], but most impressive results were achieved recently with Yb³⁺ and Tm³⁺ doping in the 1 and 2 μm spectral regions, respectively. The latter is obviously related to the close ionic radius of Lu to that of Yb and Tm (in contrast, the isostructural KGdW is more suitable for Nd-doping).

The cw output power obtained with diode pumping of the Yb:KLuW laser reached 11 W [2] while 4 W were obtained with a diode-pumped Tm:KLuW laser [3]. In both cases thermal effects were essential: in the case of Yb-doping they clamped the slope efficiency at higher pump levels while for Tm-doping the output power limit was determined by bulk damage. The high-doping levels possible in KLuW and the high absorption and emission cross sections

make this host attractive also for thin-disc laser designs employing epitaxial layers of doped KLuW on undoped KLuW substrate. Diode pumping of such an epitaxial Yb:KLuW/KLuW composite has already been demonstrated [4]; first results with Ti:sapphire laser pumping of a similar Tm:KLuW/KLuW composite have also been reported [5].

The space group of KLuW is $C2/c$ and the cell parameters are $a = 10.576(7) \text{ \AA}$, $b = 10.214(7) \text{ \AA}$, $c = 7.487(2) \text{ \AA}$, $\beta = 130.68(4)^\circ$ and $Z = 4$ [6]. Therefore, it can be expected that KLuW exhibits significant anisotropy in the physical properties, and in particular in its thermal properties, which are the main subject of the present paper.

Optical pumping of solid-state laser materials generates heat as a result of the thermalization within the multiplets, the nonradiative relaxations and the residual absorption (defects, impurities). Therefore, the knowledge of the thermal properties of any active material is essential for the design of the laser cavity and evaluation of the laser performance, especially in the high-power regime.

Heat removal engineering is one of the most important tasks in the design of high-power laser systems. The active cooling of the crystal is usually realized with a coolant flowing in contact with the crystal surface or the crystal metal holder. In the steady state, analytical solutions of the heat conduction equation are possible only for simple geometries with radial symmetry. In more complex geometries or for non-stationary thermal load, full 3-D finite element numerical simulation is necessary to analyze the thermal behavior.

The anisotropy of the thermal conductivity affects the strategies for pumping and cooling the laser crystal. The knowledge of the temperature distribution inside the crystal for different pump conditions is crucial for the design of efficient removal of the heat generated. In this work we will analyze the thermal response of the crystal to a steady state pump.

The non-uniform temperature distribution inside the laser crystal results in a distortion of the laser beam due to temperature and stress-dependent variation of the index of refraction. These changes produce thermal lensing and thermal stress induced birefringence, which depends on the thermo-optic coefficient, dn/dT , and the thermal conductivity of the material. Additionally, thermal expansion stress produces also a distortion of the flatness of the crystal faces, generating a thick-lens that also perturbs the propagation of the laser beam. In the steady state and with isotropic thermal conductivity, these effects can be compensated with a negative lens, because as a result of the parabolic radial temperature profile, the crystal behaves like a lens-like medium with positive focal length [7]. In more complicated situations (non-uniform heating, anisotropic thermal conductivity, etc), the radial temperature dependence is not parabolic and the focal length at the center of the active element is not the same as near the edges. In such cases, precise knowledge of the temperature distribution inside the crystal is needed in order to reduce the thermally induced optical distortions.

In the present work, a detailed thermal characterisation of the KLuW host will be given, with special emphasis on the anisotropy of the different parameters.

2. Crystal growth of bulk KLuW and sample preparation

KLuW exhibits polymorphic transformations. The crystallographic phase interesting for laser applications is the monoclinic one, and this phase is not the high temperature phase. As a consequence, KLuW cannot be grown directly from the melt and must be grown from high temperature solutions. The solvent used by us was $K_2W_2O_7$ and the growth method was the Top Seeded Solution Growth by Slow Cooling (TSSG-SC). The crystal growth experiments were carried out in a cylindrical vertical furnace with a Kanthal heater. An Eurotherm 903P programmable temperature controller was employed, connected to a thyristor. The single crystals of KLuW were grown using 125 cm^3 cylindrical platinum crucibles. The reagents were K_2CO_3 (Fluka, 99.0%), WO_3 (Fluka, 99.9%) and Lu_2O_3 (Aldrich, 99.9%). The solution composition was 12 mol % KLuW – 88 mol % $K_2W_2O_7$ with a weight of about 200 g. The axial temperature gradient in the solution was about 1.5 K/cm, with hot bottom. A KLuW seed with orientation along the crystallographic b -axis was located at the center of the solution

surface. The saturation temperature was determined by repeatedly measuring the dissolution/growth of the seed, with a precision of 0.01 mm. During the growth, the temperature of the solution was decreased slowly at a rate of 0.1-0.2 K/h for 20 K, depending on the crystal size required. The rotation of the crystals was maintained constant at 40 rpm for homogenisation of the solution. Finally, the crystals were removed slowly from the solution and located slightly above the solution surface, and the furnace was cooled at a rate of 25 K/h.

For thermal diffusivity measurements, plates were cut from the bulk crystals with an area of $3 \times 3 \text{ mm}^2$ and thickness of $\approx 500 \text{ }\mu\text{m}$. The plates were cut with normal along four different crystallographic directions: *a*, *b*, *c* and *c**. Each sample was first lapped and then polished to optical grade quality using Al_2O_3 powder with $1 \text{ }\mu\text{m}$ and $0.3 \text{ }\mu\text{m}$ particle size. Finally, the samples were inspected by confocal microscopy: their average roughness was 8 nm.

3. Specific heat capacity

The specific heat investigations were performed using the Specific Heat option of the Quantum Design Physical Property Measurement System, developed recently at the Institute of Physics of the Polish Academy of Sciences. In this system, a relaxation method is applied to determine the heat capacity over the temperature range from 1.9 to 385 K. The mass of the sample can range from 2 to 500 mg.

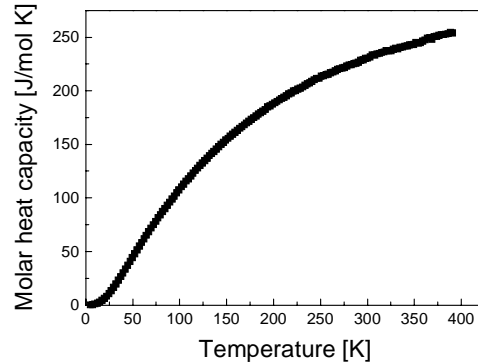


Fig. 1. Molar heat capacity of a single crystal of KLuW versus temperature

Figure 1 presents the results of the specific heat capacity measurement of KLuW. Only the phonon contribution is responsible for this dependence, because in the insulating KLuW compound no electron contribution is present and the non-magnetic Lu^{3+} ions, which are in the 1S_0 ground state, bring no magnetic and Schottky contributions. The specific heat capacity of KLuW increases with temperature. Some saturation tendency is observed above room temperature but no anomaly can be seen over the whole temperature range studied. The value of the specific heat capacity at 300 K is $C_p=0.324 \text{ J/g K}$ (molar heat capacity $\approx 230 \text{ J/mol K}$). This value agrees well with previous results reported in the literature on some isostructural KREW (RE=Gd, Y, Yb) compounds, see Table 1.

Table 1. Specific heat capacity C_p and molar heat capacity of monoclinic KREW (RE=Gd, Y, Yb and Lu)

	Molar weight [g/mol]	T [K]	C_p [J/g K]	Molar heat capacity [J/mol K]	Ref.
KGdW	691.950	300	0.363	251.2	[8]
KYW	623.650	300	0.397	247.6	[8]
KYbW	707.740	300	0.329	232.8	[9]
KLuW	709.667	300	0.324	229.9	This work

The values in the table confirm the expected tendency of decreasing specific heat capacity with the molecular weight of the compound. Hence, the doping of KLuW with Tm and Yb, will increase the molar heat capacity which means that doping could only improve the damage resistivity of the compound when subjected to laser radiation (the temperature variation in the crystal is related with the molar heat capacity).

From the low temperature part of the data in Fig. 1, the Debye temperature was determined and its value is $\theta_D=303\pm 3$ K, see Fig. 2. The Debye temperature is related to the cut-off frequency for vibrations propagating along the ionic chains established in the crystalline structure, $\omega_D = 2\pi k_B \theta_D / h$, where k_B and h are the Boltzmann and Planck constants, respectively. This frequency in combination with the average inter-atomic spacing, a_0 , determines the sound velocity in the crystal, $v = a_0 \omega_D / \pi$, considering an isotropic medium. We have evaluated these two parameters for KLuW and obtained $\omega_D = 1324 \text{ cm}^{-1}$ and $v = 3734 \text{ m/s}$. Both values obtained are lower in comparison to YAG [11]. In insulator materials, it can be assumed that only the acoustic phonon modes participate in the heat conduction process and consequently the thermal conductivity, κ , can be expressed as $\kappa = \rho v^4 / T \omega_D \gamma^2$, where ρ is the material density and γ is the Grüneisen parameter related to the covalence degree of the compound.

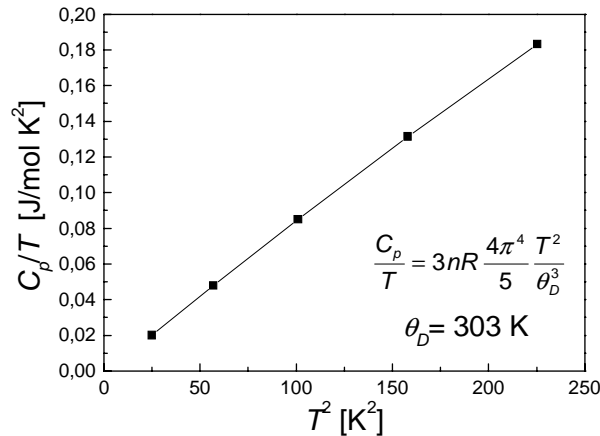


Fig. 2. Lattice component C_p/T and Debye temperature θ_D of KLuW.

The Debye temperature is also associated with the phenomena of temperature-dependent line broadening in radiative transitions, due to electron-phonon coupling [12]. For a laser line, the thermal line broadening and thermal shift are related to the gain cross section, output frequency stability, and thermal tunability of the laser [13]. Narrower spectral lines are expected for weaker impurity-phonon coupling and for host crystals with higher Debye temperature [12]. KLuW has a lower Debye temperature than YAG (303 ± 3 K against 760 K [8]) and as known for several dopants, the spectral linewidths in KLuW are broader, which is advantageous for tunable or short pulse laser operation.

4. Linear thermal expansion tensor

The unit cell parameters of KLuW were measured as a function of temperature by X-ray powder diffraction analysis using a Siemens D-5000 diffractometer (Bragg-Brentano parafocusing geometry and vertical θ - θ goniometer) equipped with a high temperature chamber (Anton-Paar HTK10). The X-ray powder diffraction patterns were recorded at

$2\theta=10-70^\circ$, size step= 0.03° , step time=5 s, and temperatures of 298, 323, 373, 473, 573, 673 and 773 K. The Fullprof software was applied to the structural model obtained for KLuW by single crystal X-ray diffraction. The powder samples were placed on a platinum holder. The linear thermal expansion coefficients in a given crystallographic direction are $\alpha=(\Delta L/\Delta T)/L_{RT}$, where L_{RT} is the initial parameter at 298 K (room temperature).

The components of the linear thermal expansion tensor, α_{ij} , can be evaluated from the slopes of the linear relationship between $(\Delta L/L_{RT})$ and temperature (ΔT) in the different crystallographic directions [14] (see Fig. 3(a)). For KLuW this procedure has already been reported elsewhere [6] and for the other KREW compounds in [15]. For the sake of completeness, the results are briefly summarized here.

Linear thermal expansion of a crystal is represented by a symmetrical second-rank tensor and if the crystal is monoclinic it has four nonzero components in the crystallo-physical frame X_{1d}/\mathbf{a} , X_{2d}/\mathbf{b} , X_{3d}/\mathbf{c}^* , where \mathbf{c}^* is a vector from the reciprocal crystallographic system. The values of the diagonal elements are $\alpha_{11}=\alpha_{10}$, $\alpha_{22}=\alpha_{010}$, and $\alpha_{33}=\alpha_{c^*}$ and from the equation $\alpha_{001}=a_i a_j \alpha_{ij}$, where a_i and a_j are the direction cosines, one can deduce α_{13} as the unique unknown quantity of the equation if α_{001} is measured.

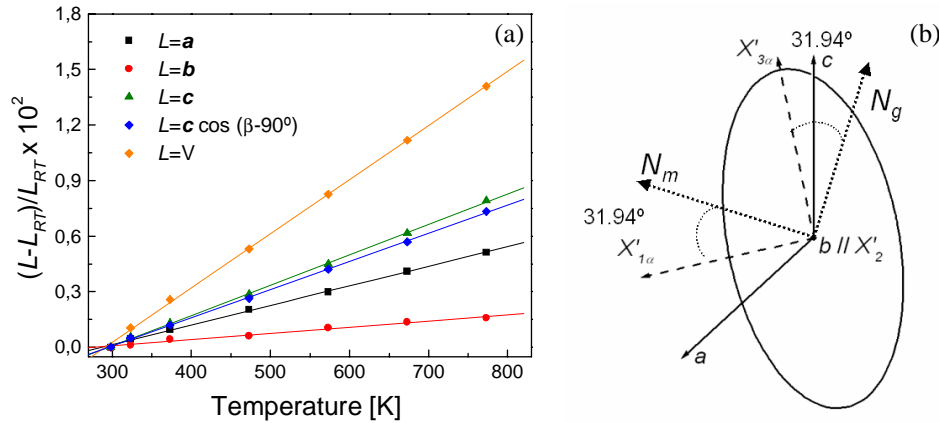


Fig. 3. Unit cell parameters evolution with temperature (a) and linear thermal expansion (b) of KLuW.

The unit cell parameters a , b and c of KLuW increase with temperature and β remains constant (Fig. 3(a)). The measured linear thermal expansion tensor components are included in Table 2. The derived value for α_{13} is $-3.15 \times 10^{-6} \text{ K}^{-1}$. Considering the linear thermal expansion of the volume, α_v , and taking into account the relations between thermal expansion and covalence as well as thermal expansion and density of weak bonds [16], one can conclude that the degree of covalence in the chemical bonds of the KREW family follows $\text{KGdW} < \text{KLuW} < \text{KYW} < \text{KYbW}$.

Table 2. Linear thermal expansion coefficients of KREW compounds (RE=Gd, Y, Yb, Lu), in units 10^{-6} K^{-1} , and some of their ratios [6,15].

	KGdW	KYW	KYbW	KLuW
α_{100}	13.6	11.0	10.5	10.6
α_{010}	2.8	1.9	2.6	3.35
α_{001}	22.8	17.8	16.3	16.3
α_{c^*}	20.5	15.3	14.8	15.1
α_{ν}	37.1	28.3	26.9	29.2
α'_{11}	10.6	8.3	8.7	8.98
α'_{22}	2.8	1.9	2.6	3.35
α'_{33}	23.4	18.0	16.6	16.72
α'_g	19.54	15.99	14.47	14.55
α'_m	14.56	10.31	9.07	11.19
α'_p	2.8	1.9	2.6	3.35
α'_g/α'_m	1.34	1.55	1.59	1.30
α'_g/α'_p	6.98	8.41	5.56	4.34
α'_m/α'_p	5.2	5.43	3.49	3.34
α'_{k1}	-	-	-	9.16
α'_{k2}	-	-	-	3.35
α'_{k3}	-	-	-	16.54

As every symmetrical tensor the linear thermal expansion satisfies an eigenvalue equation. From $\det(\alpha'_{ij} - \lambda \delta_{ij}) = 0$ one can obtain the eigenvalues α'_{ii} , shown for KLuW in the same Table 2, which are the diagonal values of the tensor expressed in the eigenframe (principal axes of the property) $X'_{1\alpha}$, $X'_{2\alpha}/b$, and $X'_{3\alpha}$. The orientation of the $X'_{1\alpha}$ and $X'_{3\alpha}$ axes in the $N_g - N_m$ principal optical plane (N_p/b , N_m , and N_g are the three principal optical axes defined from the relation between the three refractive indices, $n_p < n_m < n_g$) can be determined from the tensor equation $\alpha'_{ij} = a_{ik} a_{jl} \alpha_{kl}$, where a represents the transfer matrix from the crystallo-physical frame to the principal frame of the physical property, and the known orientation of the optical ellipsoid. As can be seen from Fig. 3(b) the ellipsoid of the linear thermal expansion is rotated by 31.94° relative to the optical ellipsoid (all frames shown are right-handed).

The values of the linear thermal expansion coefficients along the principal optical axis, calculated and included in the same Table 1, are more important in practice because normally the laser elements are cut along one of these axes. If the ratios α'_g/α'_m , α'_g/α'_p and α'_m/α'_p are taken as a measure for the linear thermal expansion anisotropy, one can see from the table that this anisotropy decreases along the KREW series. Thus, KLuW is the passive host in the KREW family with the lowest thermal expansion anisotropy. This lowest anisotropy means smallest distorting contribution from the crystal faces to the thermal lens and lowest probability of cracking for thermal reasons during the lasing process.

5. Thermal conductivity tensor

The components of the thermal diffusivity tensor (D_{ij}) have been measured using photopyroelectric calorimetry [17]. In this method the front surface of the sample is illuminated by a modulated light beam, while its rear surface is in contact with a pyroelectric detector which measures the resulting temperature oscillations. With this method, high-resolution measurements are obtained since small temperature gradients in the sample produce a good signal-to-noise ratio. In our experimental setup a 5 mW He-Ne laser modulated by an acousto-optic modulator has been used as heating source. The pyroelectric transducer was a 350 μm thick LiTaO₃ crystal with Ni-Cr electrodes plated on both surfaces. Samples were attached to the pyroelectric transducer by using an extremely thin layer of highly heat-conductive silicone grease (Dow Corning, 340 Heat Sink Compound). The photopyroelectric

current was processed by a two-phase lock-in amplifier yielding a vector signal output comprising the amplitude and phase of the signal with respect to the reference. Both sample and detector were placed inside a nitrogen bath cryostat that allows measurements in the temperature range from 77 to 500 K.

It has been demonstrated that the phase of the photopyroelectric current depends linearly on \sqrt{f} , where f is the modulation frequency. Moreover, the slope m of this linear dependence is related to the thermal diffusivity D of the sample in the direction normal to the surface through the equation [17],

$$D = \frac{\pi \ell^2}{m^2}, \quad (1)$$

where ℓ is the sample thickness. This equation is valid for opaque and thermally thick samples (i.e. ℓ larger than the thermal diffusion length $\mu = \sqrt{D/\pi f}$). Once the thermal diffusivity has been measured (D_{ref}) at a certain reference temperature (T_{ref}), the temperature is continuously varied while recording the phase of the photopyroelectric signal, at a fixed frequency. Indeed, changes in the phase are directly related to changes in the thermal diffusivity of the sample. In this way, the temperature dependence of D is given by the following expression [18]:

$$D(T) = \left(\frac{1}{\sqrt{D_{ref}}} - \frac{\Delta(T)}{\ell \sqrt{\pi f}} \right)^{-2} \quad (2)$$

where $\Delta(T) = \Psi(T) - \Psi(T_{ref})$ is the phase change for a given change in temperature.

As mentioned above, four single crystal plates of KLuW, whose surfaces are perpendicular to the \mathbf{a} , \mathbf{b} , \mathbf{c} , and \mathbf{c}^* crystallographic directions, were studied. For a better comparison, all of them had similar thickness: between 514 and 517 μm . Since KLuW is transparent at the He-Ne laser wavelength, the front surface was coated with a thin metallic layer. Several heating runs from 300 to 500 K at a rate of 0.1 K/min were performed. A modulation frequency of 8.0 Hz, high enough to ensure that the sample is thermally thick but low enough to provide a good signal-to-noise ratio, was applied.

The thermal conductivity, κ_{ij} , in crystals is also a symmetrical second-rank tensor which satisfies $\kappa_{ij} = D_{ij} \rho C_p$, where D_{ij} are the tensor components of the thermal diffusivity (m^2/s). As KLuW is monoclinic, this tensor has four nonzero components when expressed in the crystallo-physical frame $X_{1\kappa}/\mathbf{a}$, $X_{2\kappa}/\mathbf{b}$, $X_{3\kappa}/\mathbf{c}^*$. Accordingly, in order to evaluate the thermal diffusivity tensor as a function of temperature, it was measured in these four crystallographic directions. The results are plotted in Fig. 4 (a).

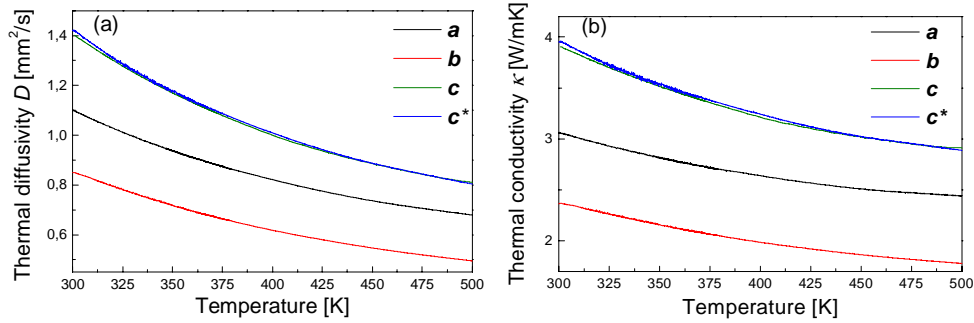
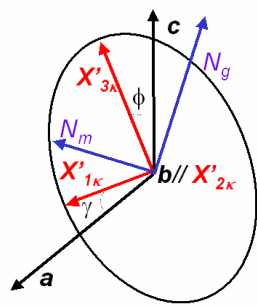


Fig. 4. Thermal diffusivity (a) and conductivity (b) of KLuW measured along the crystallographic directions a , b , c and c^* .

Using the bulk density reported in [6] and the C_p values from Fig. 1, the evolution of thermal conductivity along these four directions in the temperature range 300-500 K can be observed in Fig. 4(b). As can be seen, the thermal conductivity decreases with temperature. The transfer of heat in dielectric solids is related to a flow of phonons from hot to cold. The thermal conductivity is proportional to the lattice heat capacity, the phonon velocity, and the phonon mean free path. As shown before, the molar capacity increases with temperature, however, the phonon velocity depends only weakly on temperature. The decrease of the thermal conductivity with temperature must be related to the change of phonon mean free path, which decreases significantly with temperature [19].

From the measured value of the thermal conductivity at 300 K, in particular the diagonal elements $\kappa_{11}=\kappa_{100}$, $\kappa_{22}=\kappa_{010}$, $\kappa_{33}=\kappa_{c^*}$, (see Table 3), and the equation $\kappa_{001}=a_i a_j \kappa_{ij}$, where a_i and a_j are the direction cosines, one can deduce κ_{13} as the unique unknown quantity. The result is $\kappa_{13}=-0.33 \text{ Wm}^{-1}\text{K}^{-1}$. The eigenvalues in the principal frame of the conductivity are obtained then by diagonalization; they are also included in Table 3 and denoted by primed symbols κ'_{ii} .

At 300 K, the principal axis with maximum thermal conductivity, $X'_{3\kappa}$, was found at $\phi=22.25^\circ$ from the c axis (see Fig. 5). The principal axis $X'_{1\kappa}$ with the medium thermal conductivity coefficient is then at $\gamma=(\beta-90^\circ)-\phi=18.45^\circ$ from the a axis. In addition, once knowing the orientation of the ellipsoid (Fig. 5), it was possible to extend Table 2 with values of the linear thermal expansion along the principal thermal conductivity directions at 300 K.



Temperature [K]	ϕ°	γ°
300	22.25	18.45
400	22.10	18.60
500	18.65	22.05

Fig. 5. Thermal conductivity ellipsoid of KLuW.

Using the measured thermal conductivity values at 400 and 500 K, similar calculations gave the values $\kappa'_{11}=2.56$, $\kappa'_{22}=1.98$ and $\kappa'_{33}=3.32 \text{ Wm}^{-1}\text{K}^{-1}$, and $\kappa'_{11}=2.35$, $\kappa'_{22}=1.77$ and

$\kappa'_{33}=2.97 \text{ Wm}^{-1}\text{K}^{-1}$, at these two elevated temperatures, respectively. The rotation of the thermal conductivity tensor with temperature is summarized in Fig. 5. When the temperature increases from room temperature to 500 K, the thermal conductivity eigenvalues along κ'_{11} , κ'_{22} and κ'_{33} , decrease by 20%, 24.6% and 26.8%, respectively.

Thermal conductivity values obtained for KLuW in the present work and previously reported values for other members of the KREW family are summarized in Table 3.

Table 3. Thermal conductivity values (in units $\text{W/m}^1\text{K}^{-1}$) of KLuW and related compounds at 300K.

κ	KLuW	Yb:KLuW	KGdW	KGdW	KYW
κ'_{100}	3.06	3.11	-	2.6	-
κ'_{010}	2.36	2.55	2.6	3.8	2.7
κ'_{001}	3.90	3.98	-	3.4	-
κ'_{c^*}	3.95	-	-	-	-
κ'_{11}	2.95	3.09	-	-	-
κ'_{22}	2.36	2.55	-	-	-
κ'_{33}	4.06	4.40	-	-	-
κ'_{g}	3.59	-	-	-	-
κ'_{m}	3.41	-	-	-	-
κ'_{p}	2.36	-	-	-	-
κ'_{g}/κ'_{m}	1.05	-	-	-	-
κ'_{g}/κ'_{p}	1.52	-	-	-	-
κ'_{m}/κ'_{p}	1.44	-	-	-	-
$\kappa'_{\alpha 1}$	2.975	-	-	-	-
$\kappa'_{\alpha 2}$	2.36	-	-	-	-
$\kappa'_{\alpha 3}$	4.03	-	-	-	-
Ref.	This work	[10]	[8]	[20]	[8]

Comparing with the other KREW compounds, the thermal conductivity of KLuW is slightly lower, which could be expected taking into account the higher molar mass and the lower melting point of KLuW in comparison to the other members of the KREW family (in spite of the more compact crystal structure [21]). For 5% Yb-doped KLuW [10], slightly higher values were reported, this could mean an increase of thermal conductivity when doping with ytterbium.

6. Temperature evolution simulations

Finally, we used a finite element 3D model (Comsol Multiphysics 3.2, Comsol AB, Sweden) to compute the temperature distribution inside a KLuW laser crystal pumped in the steady state. The numerical experiment reproduces the lasing experiment carried out in a diode pumped set-up reported by Mateos *et al.* [3]. The thermal simulation was performed for a cube sample ($3 \times 3 \times 3 \text{ mm}^3$) with edges parallel to the dielectric frame of the crystal. The origin of the frame was set at the center of the cube. The model solves the 3D Fourier heat transfer equation with an anisotropic thermal conductivity tensor. We used the thermal conductivity values at room temperature, because the overheating of the whole crystal is assumed to be relatively weak.

Figure 6 shows a geometrical sketch together with the projection of the ellipsoid of the thermal conductivity on the faces of the crystal. In this figure x, y and z axes correspond to N_m , N_p and N_g directions, respectively. The crystal was divided into more than 73000 nodes using an automatic meshing. It was assumed that the crystal was pumped in a hot cylindrical volume of radius $55 \mu\text{m}$ and length 3 mm. Two different pumping strategies were considered: pumping along N_g axis (i.e. the hot area is a cylinder along z direction) and pumping along N_p

(hot area along y direction). Pumping along N_m was not considered because N_m is usually the direction of polarization preferred for pumping doped KLuW crystals [2,3].

A significant part of the pump energy is converted into heat inside the laser material. The continuous heat production was supposed to be 1 W, with homogeneous distribution over the pumped zone.

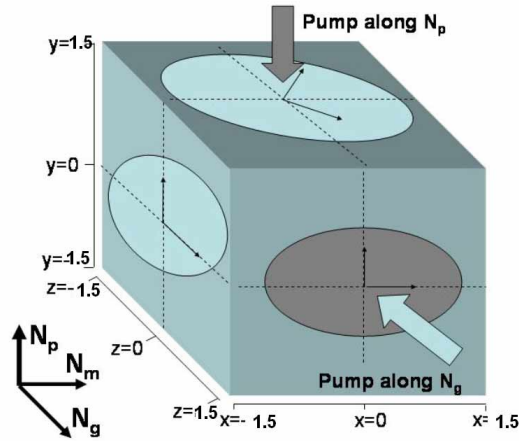


Fig.6. Geometrical sketch of the laser crystal modelled. Units are mm.

We modelled free convection (heat-transfer coefficient $h=10 \text{ Wm}^{-2}\text{K}^{-1}$) at the two pump faces of the crystal ($z=\pm 1.5 \text{ mm}$ for pump along N_g and $y=\pm 1.5 \text{ mm}$ for pump along N_p). The other four lateral faces were cooled. High-power laser crystals are normally actively cooled with coolant flowing through a metal holder in contact with the lateral surfaces. We assume that the cooling liquid, as well as the air surrounding the two pump faces, were maintained at room temperature. The forced convection coefficient varies according to the efficiency of the cooling. We considered different heat-transfer coefficients, ranging from $h=10$ (free convection, i.e. poor cooling) to $10000 \text{ Wm}^{-2}\text{K}^{-1}$ (very efficient cooling). Continuity was imposed among all internal boundaries.

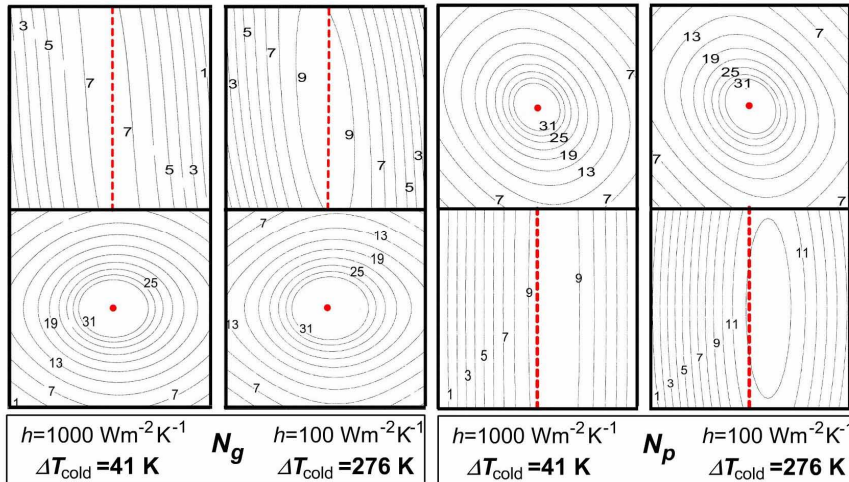


Fig.7. Overheating for pump along N_g and N_p for the faces $y=1.5$ mm (upper part) and $z=1.5$ mm (lower part).

As the coefficient of convection increases, the heat removal becomes more efficient and the temperature of the crystal decreases. We define $(\Delta T)_{\text{cold}}$ as the overheating of the coldest point of the laser crystal (relative to room temperature). This point is usually located on the edges of the crystal parallel to the pump beam, because they are the most distant from the pumping volume. For $h=10 \text{ Wm}^{-2}\text{K}^{-1}$, the coldest point of the crystal is about 1800 K above room temperature. This value decreases drastically as the efficiency of the heat removal increases. For $h=100 \text{ Wm}^{-2}\text{K}^{-1}$, $(\Delta T)_{\text{cold}}$ is 276 K and for $h=1000 \text{ Wm}^{-2}\text{K}^{-1}$, the coldest point of the crystal is only 41 K above room temperature. We found that for $h>1000 \text{ Wm}^{-2}\text{K}^{-1}$ there is no substantial decrease of $(\Delta T)_{\text{cold}}$. Figure 7 shows the overheating of the frontal ($z=1.5$ mm) and the upper side ($y=1.5$ mm) of the crystal for pump along N_g and N_p . Two intermediate cooling efficiencies ($h=100$ and $h=1000 \text{ Wm}^{-2}\text{K}^{-1}$) are displayed. $(\Delta T)_{\text{cold}}$ must be added to the overheating data to obtain the temperature in each point (relative to room temperature). The dots and lines indicate the entrance point and the path of the pump, respectively.

Figure 7 indicates that the overheating patterns are similar for both convection conditions analyzed, even though the mean temperature of the crystal decreases when convection increases. It is interesting to note that the asymmetry in the thermal conductivity tensor produces changes in the overheating of the crystal depending on the pumping strategy. For pump along N_g , the temperature distribution in the cooling faces ($y=1.5$ mm in Fig. 7) is distorted in accordance with the anisotropy of the tensor. The pumping faces ($z=1.5$ mm in Fig. 7) show a somewhat oval but smooth temperature distribution. For pump along N_p , the isotherms in the cooling faces are quasi parallels to the faces of the crystal, but the maximum temperature in these faces is displaced towards $x>0$ in the $y=1.5$ mm plane and $x<0$ in the $y=-1.5$ mm plane (not presented in Fig. 7). For these pump conditions, the pump propagates in the hottest area of the crystal, favoring the efficient removal of the generated heat. This does not happen for N_g pumping. Another advantage of N_p pumping is that both the pump and the laser beams will propagate along an isothermal zone (i.e., with low optical distortion). The non-zero value of the N_m-N_g (xz) component of the thermal conductivity tensor produces a significant tilt of the maximum temperature line, especially for weak heat removal and N_g pumping. Serious distortions can be expected then as a result of the thermo-optic effect, $dn/dT \neq 0$. Also note that for similar convection conditions, N_p pumping produces a temperature

distribution in the cooling planes slightly higher than N_g pumping, thus favoring the heat removal and reducing the thermal gradients inside the crystal.

7. Conclusions

The specific heat capacity of KLuW at 300 K is 0.324 J/gK (molar heat capacity ≈ 230 J/molK) and the Debye temperature is $\theta_D=303\pm 3$ K. Up to the maximum temperature of 385 K studied, the specific heat capacity of KLuW shows no saturation.

The anisotropy of the linear thermal expansion and thermal conductivity of monoclinic KLuW has been evaluated. The volume linear thermal expansion of KLuW is $\alpha_V=29.2 \cdot 10^{-6} \text{ K}^{-1}$ and the average anisotropy of this property is lower in KLuW than in the other members of the KREW family of monoclinic laser hosts.

The maximum thermal conductivity of KLuW at 300 K amounts to $4.06 \text{ Wm}^{-1}\text{K}^{-1}$, along the X'_{3k} direction, which is located at 22.25° from the c crystallographic direction and at 40.75° from the N_g principal optical direction. The thermal conductivity of KLuW decreases with temperature, by an average of 24% for a temperature increase of 200 K above room temperature.

A Finite Element 3D model was applied to analyze the heat transfer in the anisotropic KLuW crystal in two different crystal geometries. Depending on the pump direction, the anisotropy of the thermal conductivity tensor produces different thermal field distributions. One can conclude that pumping in the N_p direction is preferable in terms of thermal effects because the pump power is distributed along a quasi-isothermal path.

Acknowledgements

This work was supported by the EU Project DT-CRYS (NMP3-CT-2003-505580). We also acknowledge financial support from the Spanish Government by the Projects MAT2005-06354-C03-02, MAT2004-20471-E and CIT-020400-2005-14, and from the Catalan Government by the Project 2005SGR658. This work has been partially supported by the University of the Basque Country through research grant No. EHU06/24.